Appl. Math. Mech. -Engl. Ed., **42**(5), 665–676 (2021)

APPLIED MATHEMATICS AND MECHANICS (ENGLISH EDITION)

https://doi.org/10.1007/s10483-021-2726-5

Application of the homopoty analysis method to nonlinear characteristics of a piezoelectric semiconductor fiber*

Minghao ZHAO[1,2,3], Zelong MA[1], Chunsheng LU[4], Qiaoyun ZHANG[1,3,†]

1. School of Mechanics and Safety Engineering, Zhengzhou University, Zhengzhou 450001, China;
2. School of Mechanical Engineering, Zhengzhou University, Zhengzhou 450001, China;
3. Henan Key Engineering Laboratory for Anti-Fatigue Manufacturing Technology, Zhengzhou University, Zhengzhou 450001, China;
4. School of Civil and Mechanical Engineering, Curtin University, Perth 6845, Australia

(Received Dec. 13, 2020 / Revised Feb. 8, 2021)

Abstract Based on the nonlinear constitutive equation, a piezoelectric semiconductor (PSC) fiber under axial loads and Ohmic contact boundary conditions is investigated. The analytical solutions of electromechanical fields are derived by the homopoty analysis method (HAM), indicating that the HAM is efficient for the nonlinear analysis of PSC fibers, along with a rapid rate of convergence. Furthermore, the nonlinear characteristics of electromechanical fields are discussed through numerical results. It is shown that the asymmetrical distribution of electromechanical fields is obvious under a symmetrical load, and the piezoelectric effect is weakened by an applied electric field. With the increase in the initial carrier concentration, the electric potential decreases, and owing to the screening effect of electrons, the distribution of electromechanical fields tends to be symmetrical.

Key words piezoelectric semiconductor (PSC) fiber, homopoty analysis method (HAM), nonlinear analysis, asymmetrical distribution, screening effect

Chinese Library Classification O343.5
2010 Mathematics Subject Classification 74F15, 35Q74, 65H20

1 Introduction

Piezoelectric semiconductors (PSCs) that possess multiple coupling properties have many applications in smart structures and devices, such as ultrasonic amplifiers, transistors, filters, and energy harvesters[1–5]. The weak piezoelectricity of PSCs has raised concern about their semiconductor properties[6–10]. In recent years, methods have been found to strengthen the PSC piezoelectricity pivotal to high-performance sensors, nanogenerators, and solar cells[11–13]. As such, considerable attention has been given to the coupling characteristics of the piezoelectricity and transmission of carriers in PSCs.

* Citation: ZHAO, M. H., MA, Z. L., LU, C. S., and ZHANG, Q. Y. Application of the homopoty analysis method to nonlinear characteristics of a piezoelectric semiconductor fiber. *Applied Mathematics and Mechanics* (*English Edition*), **42**(5), 665–676 (2021) https://doi.org/10.1007/s10483-021-2726-5

† Corresponding author, E-mail: zhangqy@zzu.edu.cn

Project supported by the National Natural Science Foundation of China (Nos. 11702251 and 12002316)

Strain relaxation and stress concentration induced by polarization piezoelectric effects largely reduce the reliability and life of PSCs, and thus fracture problems in PSCs become more serious[14–19]. With the increase in the application demand of PSCs, many studies have been done on typical PSC structures like nanofibers, belts, and films. For example, the electromechanical fields[20], I-V characteristics[21], and energy band laws[22] of PSC fibers were analyzed under axial mechanical loads. The bending of laminated piezoelectric and PSC fibers was investigated under a transversely mechanical load[23]. Studies have also been performed on the vibration of the PSC fiber, electric potential, and carrier distribution in a PSC nanobeam driven by a time-harmonic load[24–25]. Other works have detailed the effects of temperature on the energy conversion efficiency of a PSC fiber[26], electromechanical fields in a PSC fiber[27], and electromechanical fields in a narrow plate under Schottky contact boundary conditions[28]. Furthermore, the wave propagation in a PSC plate was analyzed via the Stroh theory[29].

However, a small carrier perturbation is usually adopted to linearize the constitutive equation. Carrier perturbation becomes relatively large under a greater mechanical load or an electric field. In this case, one must analyze PSCs using the original nonlinear constitutive equation. Nonlinear constitutive and nonhomogeneous equilibrium equations for PSCs present strongly nonlinear boundary value problems, which are difficult to solve. Recently, some methods have been proposed to solve these nonlinear boundary value problems. An iterative boundary element method and the integral transformation technology were used to study a plane-strain problem with an elliptical hole in a PSC[30]. The perturbation solutions were obtained for a PSC fiber under an axial load and a PN junction between an n-type PSC and a p-type PSC[31–32]. Motivated by this, we introduce the homotopy analysis method (HAM) in this paper to analyze a PSC fiber with electric nonlinearity under coupling loads and Ohmic contact boundary conditions[33–38]. As an analytical method, the HAM is effective for weak and strong nonlinear problems and independent of small parameters. The HAM also provides freedom to choose basis functions, initial guess solutions, and auxiliary linear operators.

This paper is organized as follows. In Section 2, the basic equations and two typical boundary conditions are first described for a one-dimensional (1D) PSC fiber. Then, in Section 3, the HAM is introduced in the 1D PSC models. Next, the nonlinear characteristics of the PSC fiber are discussed via numerical results in Section 4. Finally, the main conclusions are summarized in Section 5.

2 Basic equations

As illustrated in Fig. 1, we consider a PSC fiber with length $2L$, diameter D, and c-axis along the x_3-direction. In the case of $D/2L \ll 1$, the PSC fiber can be treated as a 1D structure.

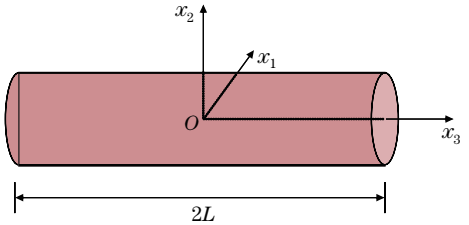

Fig. 1 Illustration of a PSC fiber with its c-axis along the x_3-direction (color online)

According to Newton's law of static equilibrium, Gauss's law of electrostatics, and the conservation of charge, the static governing equations for an n-type 1D PSC fiber are given in the Cartesian coordinates by

$$\begin{cases} \sigma_{3,3} = 0, \\ D_{3,3} = q(N_D^+ - n), \\ J_{3,3} = 0, \end{cases} \tag{1}$$

where σ_3, D_3, and J_3 are the stress, the electric displacement, and the electric current density in the x_3-direction, respectively, and q, N_D^+, and n are the unit electric charge, the donor concentration, and the electron concentration, respectively. In a natural state, N_D^+ equals the initial electron concentration n_0, and $q = 1.602 \times 10^{-19}$ C. For a 1D n-type PSC fiber, the constitutive relations can be represented as

$$\begin{cases} S_3 = s_{33}\sigma_3 + d_{33}E_3, \\ D_3 = d_{33}S_3 + \varepsilon_{33}E_3, \\ J_3 = qn\mu_{33}E_3 + qD_{33}n_{,3}, \end{cases} \tag{2}$$

where S_3 is the strain tensor, E_3 is the electric field in the x_3-direction, s_{33} is the elastic compliance, d_{33} and ε_{33} are the piezoelectric and dielectric constants, respectively, and μ_{33} and D_{33} are the mobility and the diffusion of electrons, respectively. The strain S_3 and the electric field E_3 are related to the elastic displacement u_3 and the electric potential ϕ through $S_3 = u_{3,3}$ and $E_3 = -\phi_{,3}$, respectively. By substituting u_3 and ϕ into Eq. (2), the constitutive equations can be converted to

$$\sigma_3 = \overline{c}_{33}u_{3,3} + \overline{e}_{33}\varphi_{,3}, \quad D_3 = \overline{e}_{33}u_{3,3} - \overline{\varepsilon}_{33}\varphi_{,3}, \quad J_3 = -qn\mu_{33}\varphi_{,3} + qD_{33}n_{,3}, \tag{3}$$

where the effective elastic, piezoelectric, and dielectric constants for the 1D PSC fiber are obtained through

$$\overline{c}_{33} = 1/s_{33}, \quad \overline{e}_{33} = d_{33}/s_{33}, \quad \overline{\varepsilon}_{33} = \varepsilon_{33} - d_{33}^2/s_{33}. \tag{4}$$

By substituting Eq. (3) into Eq. (1), one has

$$\begin{cases} \overline{c}_{33}u_{3,33} + \overline{e}_{33}\phi_{,33} = 0, \\ \overline{e}_{33}u_{3,33} - \overline{\varepsilon}_{33}\phi_{,33} = -q\Delta n, \\ -\mu_{33}n_{,3}\phi_{,3} - \mu_{33}n\,\phi_{,33} + D_{33}n_{,33} = 0, \end{cases} \tag{5}$$

where Δn represents the electron concentration perturbation, and $\Delta n = n - n_0$.

Furthermore, we consider the 1D PSC fiber subject to two typical boundary conditions.

Case 1:

$$\sigma(\pm L) = F_0, \quad D(\pm L) = D_0, \quad J(\pm L) = J_0, \tag{6}$$

where F_0, D_0, and J_0 are prescribed values. To make the mechanical and electric fields unique, we set $u_3(0) = 0$ and $\phi(0) = 0$.

Case 2:

$$\begin{cases} \sigma(\pm L) = F_0, \\ \phi(-L) = 0, \quad \phi(L) = V_a, \\ n(-L) = n_0, \quad n(L) = n_1, \end{cases} \tag{7}$$

where V_a and n_1 are prescribed values. Similarly, to make the mechanical field unique, we set $u_3(0) = 0$.

Obviously, the governing expressions in Eq. (5) and the boundary conditions in Eqs. (6) and (7) consist of nonlinear boundary value problems, which can be analytically solved by introducing the HAM.

3 HAM for 1D PSC models

To improve the calculation efficiency, we first simplify the governing expressions in Eq. (5) and the boundary conditions in Eqs. (6) and (7), and then solve the simplified nonlinear boundary value problems with the HAM.

3.1 HAM for Case 1

According to the static equilibrium equation in Eq. (1) and the mechanical load boundary condition in Eq. (6), we obtain $\sigma_3 = F_0$. Then, according to Eq. (3) and the unique mechanical field condition in Case 1, we have

$$u = \frac{1}{\overline{c}_{33}}(F_0 x - \overline{e}_{33}\phi). \tag{8}$$

Similarly, according to the conservation of charge equation in Eq. (1) and the electric current density boundary condition in Eq. (6), we obtain $J_3 = J_0$. By simplifying Eq. (5), we have

$$n = \frac{\overline{e}_{33}^2 + \overline{c}_{33}\overline{\varepsilon}_{33}}{\overline{c}_{33} q}\frac{\mathrm{d}^2\phi}{\mathrm{d}x^2} + n_0. \tag{9}$$

Substituting Eq. (9) and $J_3 = J_0$ into the electric current density in Eq. (3), we derive the equivalent governing equation as

$$\frac{\mathrm{d}^3\phi}{\mathrm{d}x^3} + a_1\frac{\mathrm{d}^2\phi}{\mathrm{d}x^2}\frac{\mathrm{d}\phi}{\mathrm{d}x} + a_2\frac{\mathrm{d}\phi}{\mathrm{d}x} = J_0, \tag{10}$$

where

$$a_1 = -\frac{\mu_{33}}{D_{33}}, \quad a_2 = -\frac{\overline{c}_{33} n_0 q \mu_{33}}{D_{33}(\overline{e}_{33}^2 + \overline{c}_{33}\overline{\varepsilon}_{33})}. \tag{11}$$

According to the constitutive equation of electric displacement in Eq. (3) and the electric field unique condition, we finally derive the equivalent boundary conditions as

$$\phi(0) = 0, \quad \frac{\mathrm{d}\phi}{\mathrm{d}x}(\pm L) = b, \tag{12}$$

where $b = \frac{\overline{e}_{33}F_0 - \overline{c}_{33}D_0}{\overline{e}_{33}^2 + \overline{c}_{33}\overline{\varepsilon}_{33}}$.

In the HAM, the solution to a nonlinear problem can be expressed by different basic functions. Here, we choose a polynomial basis function to express the solution to Eq. (10), that is,

$$\phi(x) = \sum_{n=0}^{+\infty} c_n x^n, \tag{13}$$

where c_n is an undetermined constant, and n is the number of polynomial terms. According to the boundary conditions in Eq. (12) and the solution to Eq. (13), we set the initial guess solution as

$$\phi_0(x) = bx, \tag{14}$$

which satisfies all the boundary conditions. According to Eqs. (10) and (14), we choose the following auxiliary linear operator:

$$L(\phi(x;p)) = \frac{\partial^3\phi(x;p)}{\partial x^3}, \tag{15}$$

where $p \in [0,1]$ is an embedding parameter. The auxiliary linear operator L satisfies

$$L(C_1x^2 + C_2x + C_3) = 0, \tag{16}$$

where C_1, C_2, and C_3 are integration constants. Then, the zeroth-order deformation equation is obtained as

$$(1-p)L(\phi(x;p) - \phi_0(x)) = phN(\phi(x;p)), \tag{17}$$

where $N(\phi(x;p))$ represents the nonlinear operator of Eq. (10), and h is a convergence-control parameter. $\phi(x;p)$ satisfies

$$\phi(0,p) = 0, \quad \frac{\partial\phi}{\partial x}(\pm L, p) = a. \tag{18}$$

Note that, at $p = 0$ and $p = 1$, we have $\phi(x;0) = \phi_0(x)$ and $\phi(x;1) = \phi(x)$, respectively, that is, as p varies from 0 to 1, $\phi(x;p)$ varies from the initial guess $\phi_0(x)$ to the true solution $\phi(x)$. Expanding $\phi(x)$ in a Taylor series with respect to p yields

$$\phi(x;p) = \phi_0(x) + \sum_{m=1}^{+\infty} \phi_m(x) p^m, \tag{19}$$

where

$$\phi_m(x) = \frac{1}{m!} \frac{\partial^m}{\partial p^m} \phi(x;p)|_{p=0}\,. \tag{20}$$

When the auxiliary linear operator L, the initial guess solution ϕ_0, and the convergence-control parameter h are properly chosen, the series in Eq. (19) converges at $p = 1$ and the homotopic series solution can be expressed as

$$\phi(x) = \phi_0(x) + \sum_{m=1}^{+\infty} \phi_m(x). \tag{21}$$

By differentiating Eq. (17) m times with respect to the embedding parameter p and dividing Eq. (17) by $m!$, an m-order deformation equation with $p = 0$ is obtained as

$$L(\phi_m(x) - \chi_m \phi_{m-1}(x)) = hR_m(\phi_{m-1}, x), \tag{22}$$

where

$$R_m(\phi_{m-1}, x) = \frac{1}{(m-1)!} \frac{\partial^{m-1}}{\partial p^{m-1}} N(\phi(x;p))|_{p=0}\,, \tag{23a}$$

$$\chi_m = \begin{cases} 0, & m \leqslant 1, \\ 1, & m > 1. \end{cases} \tag{23b}$$

The solution to Eq. (22) can be expressed as

$$\phi_m(x) = \phi_m^*(x) + C_1 x^2 + C_2 x + C_3, \tag{24}$$

where

$$\phi_m^*(x) = \chi_m \phi_{m-1}(x) + L^{-1}(hR(\phi_{m-1}, x)), \tag{25}$$

and L^{-1} is the inverse operator of L.

Based on the solution of the electric field ϕ, we can use the relationships in Eqs. (8) and (9) to obtain the elastic displacement u and the electron concentration n. Then, by substituting u and ϕ into Eq. (3), the electric displacement D_3 is determined.

The higher order expressions of electric potential ϕ, elastic displacement u_3, and electron concentration perturbation Δn can be easily derived with MATHEMATICA (Version 10.2, Wolfram Research). For example, the zeroth- and first-order solutions of ϕ, u_3, and Δn are

$$\phi_0(x) = ax, \quad u_{30}(x) = \frac{F_0 x - a e_{33} x}{c_{33}}, \quad \Delta n_0(x) = 0, \tag{26a}$$

$$\begin{cases} \phi_1(x) = ax + \dfrac{ab_2 hx(x^2 - 3L^2)}{6}, \\ u_{31}(x) = \dfrac{F_0 x}{c_{33}} - \dfrac{a e_{33} x \left(a + b_2 h(x^2 - 3L^2)\right)}{6c_{33}}, \\ \Delta n_1(x) = \dfrac{ab_2 hx(e_{33}^2 + c_{33}\varepsilon_{33})}{c_{33} q}. \end{cases} \tag{26b}$$

3.2 HAM for Case 2

Similarly, for a PSC fiber under an Ohmic contact boundary condition in Eq. (7), Eq. (5) can be finally simplified as

$$\frac{\mathrm{d}^4\phi}{\mathrm{d}x^4}+a_1\frac{\mathrm{d}^3\phi}{\mathrm{d}x^4}\frac{\mathrm{d}\phi}{\mathrm{d}x}+a_1\frac{\mathrm{d}^2\phi}{\mathrm{d}x^2}\frac{\mathrm{d}^2\phi}{\mathrm{d}x^2}+a_2\frac{\mathrm{d}^2\phi}{\mathrm{d}x^2}=0, \tag{27}$$

where a_1 and a_2 are the same as in Eq. (10). The boundary condition in Eq. (7) can be converted to

$$\begin{cases}\phi(-L)=0,\\ \phi(L)=V_a,\\ \dfrac{\mathrm{d}^2\phi}{\mathrm{d}x^2}(-L)=0,\\ \dfrac{\mathrm{d}^2\phi}{\mathrm{d}x^2}(L)=\dfrac{q\overline{c}_{33}n_1}{\overline{e}_{33}^2+\overline{c}_{33}\overline{\varepsilon}_{33}}.\end{cases} \tag{28}$$

Then, we apply the HAM to solve Eq. (27) with the boundary condition in Eq. (28). We also choose the simple polynomial form for the basic functions, and the initial guess solution to Eq. (27) and the auxiliary linear operator can be represented, respectively, as

$$\phi_0(x)=c_1x^3+c_2x^2+c_3x+c_4,\quad L(\phi(x;p))=\frac{\partial^4\phi(x;p)}{\partial x^4}, \tag{29}$$

where

$$\begin{cases}c_1=\dfrac{q\overline{c}_{33}n_1}{12(\overline{e}_{33}^2+\overline{c}_{33}\overline{\varepsilon}_{33})L},\quad c_2=\dfrac{q\overline{c}_{33}n_1}{4(\overline{e}_{33}^2+\overline{c}_{33}\overline{\varepsilon}_{33})},\\ c_3=\dfrac{6(\overline{e}_{33}^2+\overline{c}_{33}\varepsilon_{33})V_a-q\overline{c}_{33}n_1L^2}{12(\overline{e}_{33}^2+\overline{c}_{33}\overline{\varepsilon}_{33})L},\quad c_4=\dfrac{2(\overline{e}_{33}^2+\overline{c}_{33}\overline{\varepsilon}_{33})V_a-q\overline{c}_{33}n_1L^2}{4(\overline{e}_{33}^2+\overline{c}_{33}\overline{\varepsilon}_{33})L}.\end{cases} \tag{30}$$

Finally, with the same solution procedure, we can derive a homotopic series solution to Eq. (27). Similarly, The higher order expressions of ϕ, u_3, and Δn can be easily derived with MATHEMATICA (Version 10.2, Wolfram Research). The zeroth- and first-order solutions of ϕ, u_3, and Δn are

$$\phi_0(x)=d+cx+bx^2+ax^3,\quad u_{30}(x)=\frac{F_0x}{c_{33}},\quad \Delta n_0(x)=0, \tag{31a}$$

$$\begin{cases}\phi_1(x)=ax^3+bx^2+cx+d+\dfrac{h(3ab_1c+2b^2b_1+bb_2)(5L^4-6L^2x^2+x^4)}{12}\\ \qquad+\dfrac{3a^2b_1h(14L^6-15L^4x^2+x^6)}{20}+\dfrac{ah(b_2+6bb_1)(7L^4-10L^2x^2+3x^4)x}{60},\\ u_{31}(x)=\dfrac{x(F_0-ce_{33}-be_{33}x-e_{33}ax^2)}{c_{33}}-\dfrac{e_{33}h(3cab_1+2b^2b_1+bb_2)(x^2-6L^2)x^2}{12c_{33}}\\ \qquad-\dfrac{e_{33}ahx((6bb_1+b_2)(7L^4-10L^2x^2+3x^4)+9b_1x(x^4-15L^4))}{60c_{33}},\\ \Delta n_1(x)=\dfrac{(e_{33}^2+c_{33}\varepsilon_{33})(2b+6ax)}{c_{33}q}-\dfrac{9a^2b_1h(e_{33}^2+c_{33}\varepsilon_{33})(L^4-x^4)}{2c_{33}q}\\ \qquad-\dfrac{h(e_{33}^2+c_{33}\varepsilon_{33})(b(2bb_1+b_2)+2a(6bb_1x+b_2x+3b_1c))(L^2-x^2)}{c_{33}q}.\end{cases} \tag{31b}$$

4 Numerical results and discussion

In numerical studies, a ZnO fiber is selected, and the length $2L$ is set to be 1.2 μm. Moreover, its material constants are listed in Table 1. In the following calculation, we use the HAM to analyze the PSC fiber under the boundary conditions of Cases 1 and 2 with MATHEMATICA (Version 10.2, Wolfram Research).

Table 1 Material constants of the ZnO fiber used in numerical studies

Property	Parameter	Value	Unit
Elastic compliance	s_{33}	6.94×10^{-12}	$\mathrm{m^2\cdot N^{-1}}$
Piezoelectric constant	d_{33}	11.67×10^{-12}	$\mathrm{C\cdot N^{-1}}$
Dielectric constant	ε_{33}	1.12×10^{-10}	$\mathrm{F\cdot m^{-1}}$
Electron mobility	μ_{33}	0.02	$\mathrm{m^2\cdot V^{-1}\cdot s^{-1}}$
Diffusion constant	D_{33}	$5.186\ 5\times10^{-4}$	$\mathrm{m^2\cdot s^{-1}}$

4.1 Convergence analysis

It has been proved that there exists a region in the h-curves of quantities of a nonlinear problem that guarantee the convergence of homotopic series solutions[33]. Therefore, we need to plot the h-curves of extended displacements including $u_3(x)$, $\phi(x)$, and $\Delta n(x)$ to determine the effective regions. Here, we take the boundary condition (Case 1) as an example to illustrate the choice of h and the convergence of homotopic series solutions.

Next, we set the mechanical load F_0, the electric displacement D_0, the electric current density J_0, and the initial electron concentration n_0 to be 1×10^6 Pa, 1×10^{-2} $\mathrm{C\cdot m^{-2}}$, 1×10^{-5} $\mathrm{A\cdot m^{-2}}$, and 1×10^{20} $\mathrm{m^{-3}}$, respectively. As shown in Fig. 2, the effective region of h is from -0.9 to -0.15. Therefore, we choose $h=-0.6$ to derive the series solutions.

Here, it is worth noting that, as shown in Fig. 3, the homotopic series solutions are well consistent with those obtained by COMSOL. As listed in Table 2, the elastic displacement u_3 and the electric potential ϕ converge faster than the electron concentration perturbation Δn.

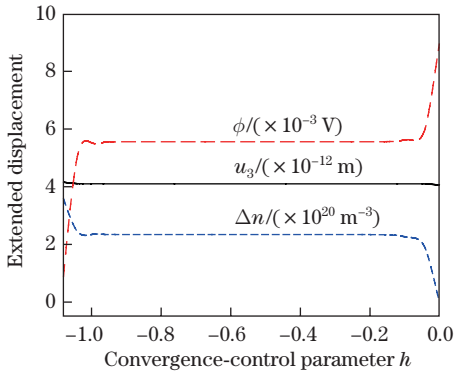

Fig. 2 h-curves of the right endpoint $x_3=L$ for different extended displacements, including the elastic displacement u_3, the electric potential ϕ, and the electron concentration perturbation Δn (color online)

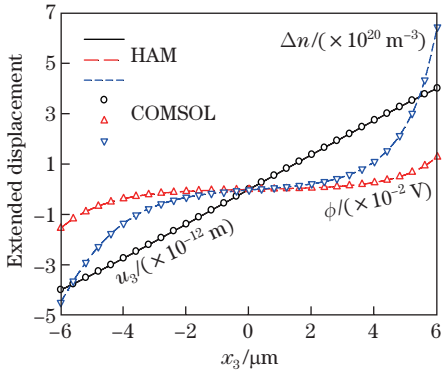

Fig. 3 Comparison of the homotopic series solutions of the displacement u_3, the electric potential ϕ, and the electron concentration perturbation Δn along the fiber by the HAM (lines) with those obtained by COMSOL (symbols) (color online)

4.2 Effects of the mechanical load

Under the boundary condition of Case 1, assume that the PSC fiber is subject to an axial mechanical load F_0. The electric displacement, the electric current density, and the initial electron concentration are fixed as $D_0=0$ $\mathrm{C\cdot m^{-2}}$, $J_0=0$ $\mathrm{A\cdot m^{-2}}$, and $n_0=1\times10^{20}$ $\mathrm{m^{-3}}$, respectively.

Table 2 Convergent results for the elastic displacement u_3, the electric potential ϕ, and the electron concentration perturbation Δn at the right endpoint $x_3 = L$ when $h = -0.6$

m	u_3/m	ϕ/V	Δn/m^{-3}
0	$4.059\,626\times10^{-12}$	$8.949\,989\times10^{-3}$	0
3	$4.099\,107\times10^{-12}$	$5.565\,919\times10^{-3}$	$2.291\,146\times10^{20}$
6	$4.099\,192\times10^{-12}$	$5.558\,676\times10^{-3}$	$2.335\,484\times10^{20}$
9	$4.099\,193\times10^{-12}$	$5.558\,557\times10^{-3}$	$2.337\,900\times10^{20}$
12	$4.099\,193\times10^{-12}$	$5.558\,552\times10^{-3}$	$2.338\,041\times10^{20}$
15	$4.099\,193\times10^{-12}$	$5.558\,551\times10^{-3}$	$2.338\,049\times10^{20}$
18	$4.099\,193\times10^{-12}$	$5.558\,551\times10^{-3}$	$2.338\,049\times10^{20}$

Normally, a small electron concentration perturbation is assumed[14–28]. The constitutive relation between the electric current density J_3 and the electron concentration n is treated as a linear relation, that is,

$$J_3 = qn_0\mu_{33}E_3 + qD_{33}n_{,3}. \tag{32}$$

However, as shown in Fig. 4, the differences in ϕ, Δn, and D_3 based on nonlinear and linear constitutive relations become more obvious as F_0 increases. Moreover, the electron concentration perturbation Δn near both ends of the fiber is larger than the initial electron concentration n_0. In this case, the assumption of small electron concentration perturbation is not applicable,

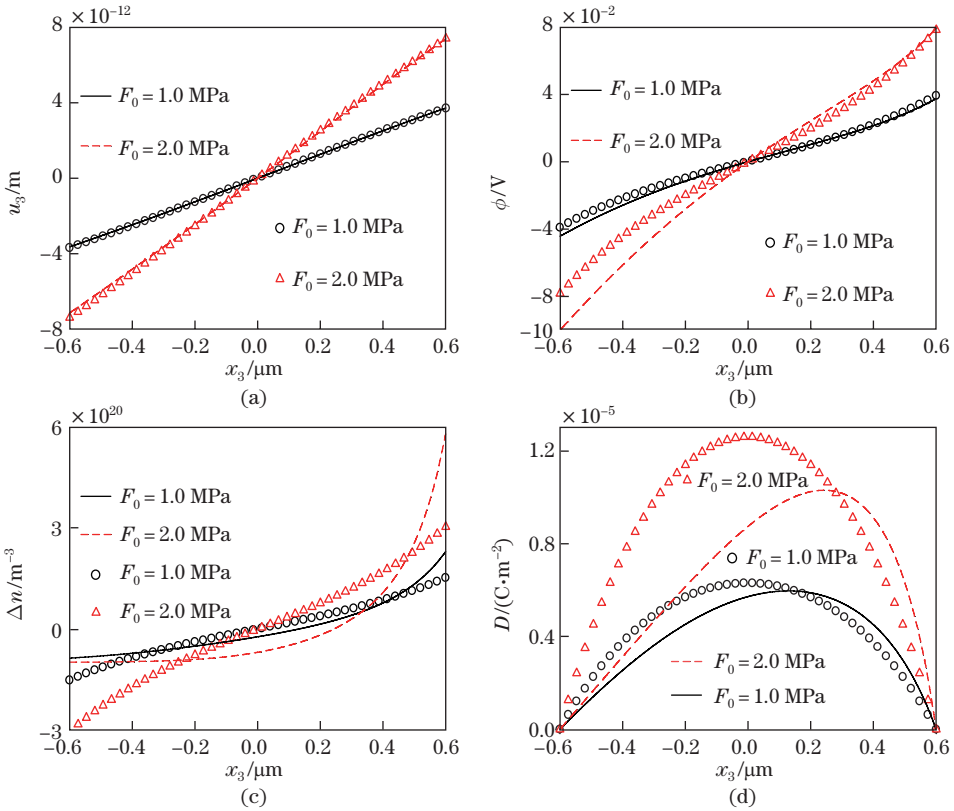

Fig. 4 (a) Elastic displacement u_3, (b) electric potential ϕ, (c) electron concentration perturbation Δn, and (d) electric displacement D_3 along the fiber length under different mechanical loads F_0. Curves are the nonlinear solutions obtained by the HAM, and symbols represent linear solutions (color online)

and the nonlinear constitutive relation must be adopted. At the same time, nonlinear solutions lose symmetry or anti-symmetry when an axial load is large, owing to the electric nonlinearity (see Fig. 4).

4.3 Effects of the applied electric field

Consider a PSC fiber under the Ohmic contact boundary condition in Eq. (7). The mechanical load, the initial electron concentration, and the electron concentration at its right end are fixed as $F_0 = 1 \times 10^6$ Pa, $n_0 = 1 \times 10^{20}$ m^{-3}, and $n_1 = 1.01 \times 10^{20}$ m^{-3}, respectively, and the electric potential V_a at the right end is taken as -0.05 V, 0 V, and 0.05 V.

Under the Ohmic contact boundary condition, the elastic displacement u_3 and the electric potential ϕ are linearly distributed. However, the electron concentration perturbation Δn is nonlinearly distributed, and the electric displacement D_3 and electric current density J_3 are uniformly distributed, as shown in Fig. 5. The distribution of Δn is nonlinear, because the two ends are fixed, and electrons spontaneously move to the positive potential end.

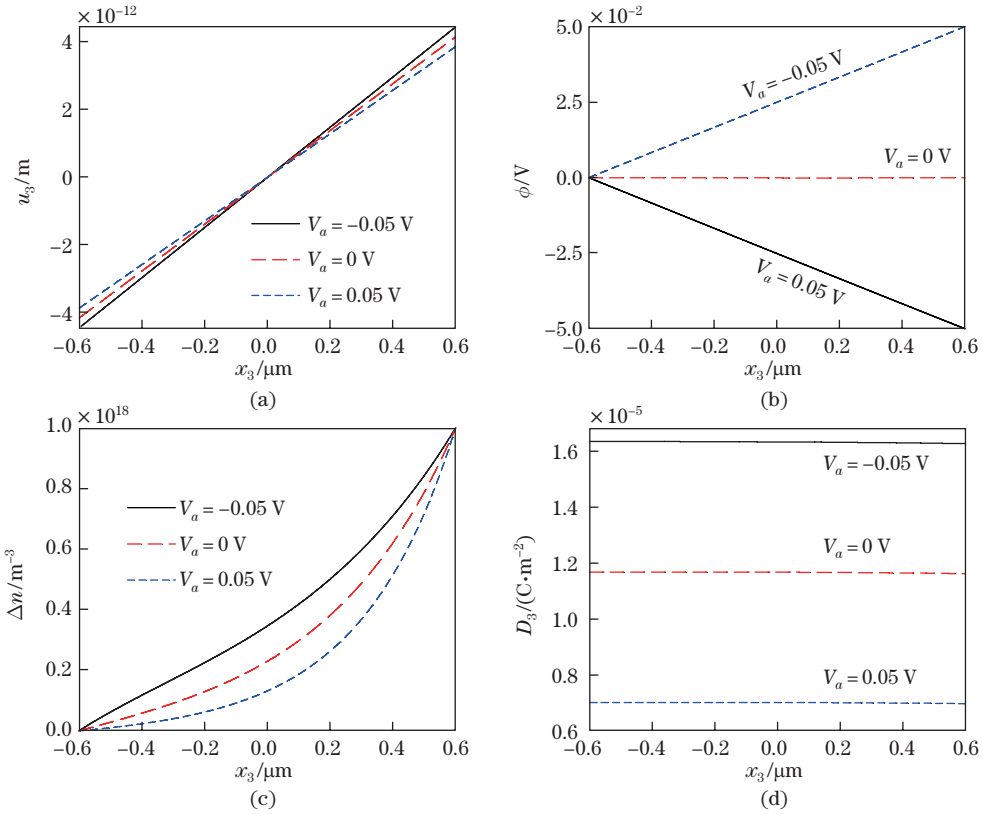

Fig. 5 (a) Elastic displacement u_3, (b) electric potential ϕ, (c) electron concentration perturbation Δn, and (d) electric displacement D_3 along the fiber length under different electric potentials V_a (color online)

4.4 Effects of the initial electron concentration

Similarly, consider a PSC fiber under the boundary condition in Eq. (6) and subject to an axial mechanical load F_0. The mechanical load, electric displacement, and electric current density are fixed as $F_0 = 2$ MPa, $D_0 = 0$ C·m^{-2}, and $J_0 = 0$ A·m^{-2}, respectively.

As shown in Fig. 6, the electric field in the fiber gradually decreases as the initial electron concentration n_0 increases owing to the screening effect of electrons. As such, the elastic displacement u_3 increases with increasing n_0. As n_0 increases, there are more electrons to screen the polarization charge, and the electric nonlinearity becomes weak. Therefore, u_3, ϕ, Δn, and D_3 tend to be symmetrical or anti-symmetrical when n_0 is high enough.

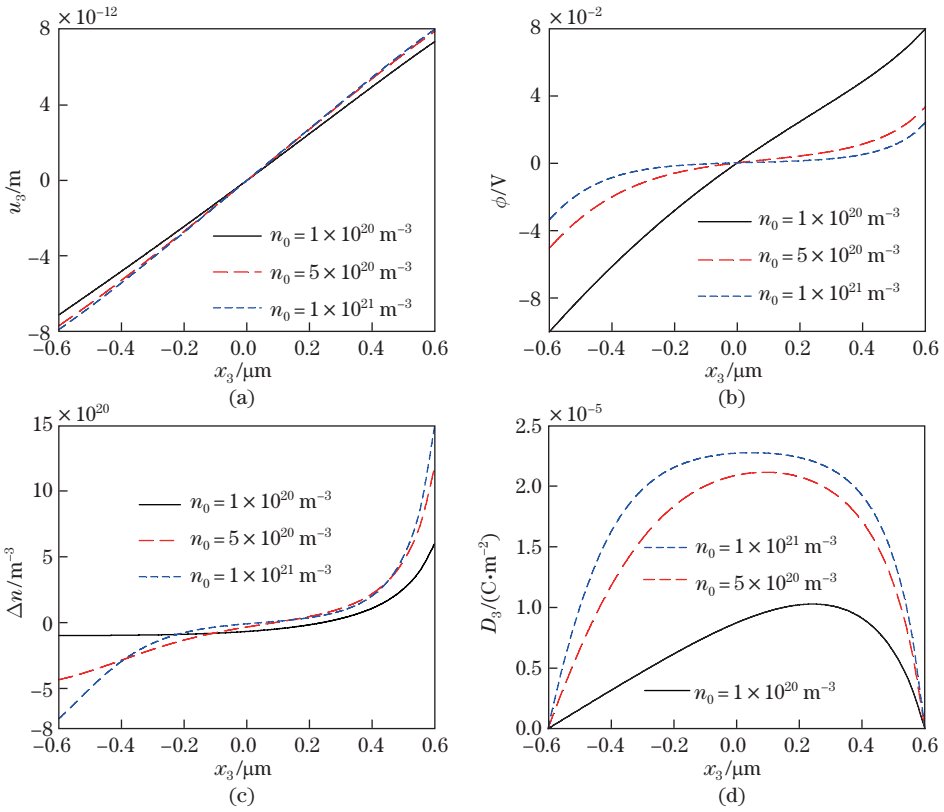

Fig. 6 (a) Elastic displacement u_3, (b) electric potential ϕ, (c) electron concentration perturbation Δn, and (d) electric displacement D_3 along the fiber length under different values of the initial electron concentration n_0 (color online)

5 Conclusions

In this paper, we have successfully derived the analytical solutions to 1D nonlinear problems in PSCs under two boundary conditions by the HAM. The main results from numerical studies can be summarized as follows.

(I) The linear theory is distorted under sufficiently large mechanical loads, and thus the original nonlinear constitutive relationship must be adopted for analyzing the electromechanical fields in PSCs.

(II) The asymmetry of an electromechanical field caused by electric nonlinearity becomes more obvious with the increase in the applied mechanical load.

(III) In the case of a high initial electron concentration, the screening effect of electrons plays a major role in distributions of electromechanical fields. As the initial electron concentration increases, the electromechanical fields tend to be symmetric or anti-symmetric.

Finally, it is expected that the HAM can be extended to solve two-dimensional and three-dimensional nonlinear problems in PSCs.

References

[1] HICKERNELL, F. S. The piezoelectric semiconductor and acoustoelectronic device development in the sixties. *IEEE Transactions on Ultrasonics, Ferroelectrics, and Frequency Control*, **52**(5), 737–745 (2005)

[2] QIN, Y., WANG, X. D., and WANG, Z. L. Microfibre-nanowire hybrid structure for energy scavenging. *nature*, **451**(7180), 809–813 (2008)

[3] LIU, Y., YANG, Q., ZHANG, Y., YANG, Y. Z., and WANG, Z. L. Nanowire piezo-phototronic photodetector: theory and experimental design. *Advance Materials*, **24**(11), 1410–1417 (2012)

[4] WANG, Z. L. Strain-gated piezotronic transistors based on vertical zinc oxide nanowires. *ACS Nano*, **6**(5), 3760–3766 (2012)

[5] WANG, Z. L. Piezopotential gated nanowire devices: piezotronics and piezo-phototronics. *Nano Today*, **5**(6), 540–552 (2010)

[6] HUTSON, A. R. and WHITE, D. L. Elastic wave propagation in piezoelectric semiconductors. *Journal of Applied Physics*, **33**(1), 40–47 (1962)

[7] GAVINI, A. and CARDONA, M. Modulated piezoreflectance in semiconductor. *Physical Review B*, **1**(2), 672–682 (1970)

[8] CHATTOPADHYAY, D. Piezoelectric and deformation potential acoustic scattering mobility of a two-dimensional electron gas in quantum wells. *Physica Status Solidi* (*B*), **135**(1), 409–413 (2010)

[9] ZHANG, X. B., TALIERCIO, T., KOLLIAKOS, S., and LEFEBVRE, P. Influence of electron-phonon interaction on the optical properties of III nitride semiconductors. *Journal of Physics*: *Condensed Matter*, **13**(32), 7053–7074 (2001)

[10] SAKAI, K., FUKUYAMA, A., TOYODA, T., and IKARI, T. Piezoelectric photothermal spectra of Co doped ZnO semiconductor. *Japanese Journal of Applied Physics*, **41**(5), 3371–3373 (2002)

[11] HE, J. H., HSIN, C. L., LIU, J., CHEN, L. J., and WANG, Z. L. Piezoelectric gated diode of a single ZnO nanowire. *Advanced Materials*, **19**(6), 781–784 (2007)

[12] ZHOU, J., GU, Y. D., HU, Y. F., MAI, W. J., YEH, P. H., BAO, G., SOOD, A. K., POLLA, D. L., and WANG, Z. L. Gigantic enhancement in response and reset time of ZnO UV nanosensor by utilizing Schottky contact and surface functionalization. *Applied Physics Letters*, **94**(19), 191103 (2009)

[13] KO, S. H., LEE, D., KANG, H. W., NAM, K. H., YEO, J. Y., HONG, S. J., GRIGOROPOULOS, C. P., and SUNG, H. J. Nanoforest of hydrothermally grown hierarchical ZnO nanowires for a high efficiency dye-sensitized solar cell. *Nano Letters*, **11**(2), 666–671 (2011)

[14] YANG, J. S. An anti-plane crack in a piezoelectric semiconductor. *International Journal of Fracture*, **136**(1-4), L27–L32 (2005)

[15] HU, Y. T., ZENG, Y., and YANG, J. S. A mode III crack in a piezoelectric semiconductor of crystals with 6 mm symmetry. *International Journal of Solids and Structures*, **44**, 3928–3938 (2007)

[16] SLADEK, J., SLADEK, V., PAN, E., and WUNSCHE, M. Fracture analysis in piezoelectric semiconductor under a thermal load. *Engineering Fracture Mechanics*, **126**, 27–39 (2014)

[17] ZHAO, M. H., PAN, Y. B., FAN, C. Y., and XU, G. T. Extended displacement discontinuity method for analysis of cracks in 2D piezoelectric semiconductors. *International Journal of Solids and Structures*, **94-95**, 50–59 (2016)

[18] FAN, C. Y., YAN, Y., XU, G. T., and ZHAO, M. H. Piezoelectric-conductor iterative method for analysis of cracks in piezoelectric semiconductors via the finite element method. *Engineering Fracture Mechanics*, **165**, 183–196 (2016)

[19] ZHANG, Q. Y., FAN, C. Y., XU, G. T., and ZHAO, M. H. Iterative boundary element method for crack analysis of two-dimensional piezoelectric semiconductor. *Engineering Analysis with Boundary Elements*, **83**, 87–95 (2017)

[20] ZHANG, C. L., WANG, X. Y., CHEN, W. Q., and YANG, J. S. An analysis of the extension of a ZnO piezoelectric semiconductor nanofiber under an axial force. *Smart Materials and Structures*, **26**(2), 025030 (2017)

[21] LUO, Y. X., ZHANG, C. L., CHEN, W. Q., and YANG, J. S. An analysis of PN junctions in piezoelectric semiconductors. *Journal of Applied Physics*, **122**(20), 204502 (2017)

[22] YANG, W. L., HU, Y. T., and YANG, J. S. Transient extensional vibration in a ZnO piezoelectric semiconductor nanofiber under a suddenly applied end force. *Materials Research Express*, **6**(2), 025902 (2019)

[23] LUO, Y. X., ZHANG, C. L., CHEN, W. Q., and YANG, J. S. Piezopotential in a bended composite fiber made of a semiconductive core and of two piezoelectric layers with opposite polarities. *Nano Energy*, **54**, 341–348 (2018)

[24] WANG, G. L., LIU, J. X., and LIU, X. L. Extensional vibration characteristics and screening of polarization charges in a ZnO piezoelectric semiconductor nanofiber. *Journal of Applied Physics*, **124**(9), 095402 (2018)

[25] DAI, X. Y., ZHU, F., QIAN, Z. H., and YANG, J. S. Electric potential and carrier distribution in a piezoelectric semiconductor nanowire in time-harmonic bending vibration. *Nano Energy*, **43**, 22–28 (2018)

[26] JIN, Z. H. and YANG, J. S. Analysis of a sandwiched piezoelectric semiconducting thermoelectric structure. *Mechanics Research Communications*, **98**, 31–36 (2019)

[27] CHENG, R. R., ZHANG, C. L., CHEN, W. Q., and YANG, J. S. Temperature effects on PN junctions in piezoelectric semiconductor fibers with thermoelastic and pyroelectric couplings. *Journal of Electronic Materials*, **49**(5), 3140–3148 (2020)

[28] ZHAO, M. H., YANG, C. H., FAN, C. Y., and ZHANG, Q. Y. A shooting method for nonlinear boundary value problems in a thermal piezoelectric semiconductor plate. *Zeitschrift für Angewandte Mathematik und Mechanik*, **100**(12), e201900302 (2020)

[29] TIAN, R., LIU, J. X., PAN, E., and WANG, Y. S. SH waves in multilayered piezoelectric semiconductor plates with imperfect interfaces. *European Journal of Mechanics-A/Solids*, **81**, 103961 (2020)

[30] ZHAO, M. H., ZHANG, Q. Y., and FAN, C. Y. An efficient iteration approach for nonlinear boundary value problems in 2D piezoelectric semiconductor. *Applied Mathematical Modelling*, **74**, 170–183 (2019)

[31] YANG, G. Y., DU, J. K., WANG, J., and YANG, J. S. Extension of piezoelectric semiconductor fiber with consideration of electrical nonlinearity. *Acta Mechanica*, **229**(11), 4663–4676 (2018)

[32] GUO, M. K., LI, Y., QIN, G. S., and ZHAO, M. H. Nonlinear solutions of PN junctions of piezoelectric semiconductors. *Acta Mechanica*, **230**, 1825–1841 (2019)

[33] LIAO, S. J. *Beyond Perturbation*: *Introduction to the Homotopy Analysis Method*, CRC Press, Boca Raton (2004)

[34] DMMAIRRY, G. and FAZELI, M. Homotopy analysis method to determine the fin efficiency of convective straight fins with temperature-dependent thermal conductivity. *Communications in Nonlinear Science and Numerical Simulation*, **14**(2), 489–499 (2009)

[35] GAO, L. M., WANG, J., ZHONG, Z., and DU, J. K. An analysis of surface acoustic wave propagation in functionally graded plates with homotopy analysis method. *Acta Mechanica*, **208**, 249–258 (2009)

[36] WU, R. X., WANG, J., DU, J. K., HUANG, D. J., YAN, W., and HU, Y. T. An analysis of nonlinear vibrations of coupled thickness-shear and flexural modes of quartz crystal plates with the homotopy analysis method. *IEEE Transactions on Ultrasonics*, *Ferroelectrics*, *and Frequency Control*, **59**(1), 30–39 (2012)

[37] WU, R. X., WANG, J., DU, J. K., HU, Y. T., and HU, H. P. Solutions of nonlinear thickness-shear vibrations of an infinite isotropic plate with the homotopy analysis method. *Numerical Algorithms*, **59**, 213–226 (2012)

[38] LIN, X., HUANG, Y., ZHAO, Y., and WANG, T. S. Large deformation analysis of a cantilever beam made of axially functionally graded material by homotopy analysis method. *Applied Mathematics and Mechanics* (*English Edition*), **40**(10), 1375–1386 (2019) https://doi.org/10.1007/s10483-019-2515-9